



LAWRENCE  
LIVERMORE  
NATIONAL  
LABORATORY

# Calculating the dynamics of High Explosive Violent Response (HEVR) after ignition

John E. Reaugh

October 20, 2008

## **Disclaimer**

---

This document was prepared as an account of work sponsored by an agency of the United States government. Neither the United States government nor Lawrence Livermore National Security, LLC, nor any of their employees makes any warranty, expressed or implied, or assumes any legal liability or responsibility for the accuracy, completeness, or usefulness of any information, apparatus, product, or process disclosed, or represents that its use would not infringe privately owned rights. Reference herein to any specific commercial product, process, or service by trade name, trademark, manufacturer, or otherwise does not necessarily constitute or imply its endorsement, recommendation, or favoring by the United States government or Lawrence Livermore National Security, LLC. The views and opinions of authors expressed herein do not necessarily state or reflect those of the United States government or Lawrence Livermore National Security, LLC, and shall not be used for advertising or product endorsement purposes.

This work performed under the auspices of the U.S. Department of Energy by Lawrence Livermore National Laboratory under Contract DE-AC52-07NA27344.

# Calculating the dynamics of High Explosive Violent Response (HEVR) after ignition

John E. Reaugh

## 1. Background

We are developing models to describe the circumstances when molecular and composite explosives undergo a rapid release of energy without detonating, and to describe the evolution of the energy release. The models also apply to the behavior of rocket propellants subject to mechanical insult, whether for accidents (Hazards) or the suite of standardized tests used to assess whether the system can be designated an Insensitive Munition (IM). In the applications described here, we are studying a UK-developed HMX (1,3,5,7-tetranitro-1,3,5,7-tetraazacyclooctane) explosive, which is 91% by weight HMX and 9% binder-plasticizer.

Most explosives and propellants, when subjected to a mechanical insult such as a drop or impact that is well below the threshold for detonation, have been observed to react. In some circumstances the reaction can be violent. This behavior is known as High Explosive Violent Response (HEVR). Fundamental to our model is the observation that the mechanical insult produces damage in a volume of the explosive near the trajectory of the impactor. The damage is manifest as surface area through the creation of cracks and fragments, and also as porosity through the separation of crack faces and isolation of the fragments. Open porosity permits a flame to spread easily and so ignite the newly formed surface area. The additional surface area leads to a direct increase in the mass-burning rate. As the kinetic energy and power of the insult increases, the degree of damage and the volume of damage both increase. Upon a localized ignition, the flame spreads to envelop the damaged volume, and the pressure rises at an accelerated rate until neither mechanical strength nor inertial confinement can successfully contain the pressure. The confining structure begins to expand. This reduces the pressure and may even extinguish the flame. Both the mass of explosive involved and the rate at which the gas is produced contribute to each of several different measures of violence. Such measures include damage to the confinement, the velocity and fragment size distributions from what was the confinement, and air blast.

In the first phase (advisory) model described in [1], the surface to volume ratio and the ignition parameter are calibrated by comparison with experiments using the UK explosive. In order to achieve the second phase (interactive) model, and so calculate the pressure developed and the velocity imparted to the confinement, we need to calculate the spread of the ignition front, the subsequent burn behavior behind that front, and the response of unburned and partially burned explosive to pressurization. A preliminary model to do such calculations is described here.

## 2. Computational test vehicle

We sought a simple computational test vehicle that could be used for examining the sensitivity of the pressure development in the damaged explosive to a variety of parameters. For our purpose, it was convenient to use a sphere of explosive surrounded

by a spherical shell. This geometry is well behaved, in that with modest rates of pressure increase, the shell expands uniformly rather than localizing the strain in what would become the region of first fracture. We note that when the ignition point is moved away from the center of the sphere, the strain does localize in the wall at the point farthest from the ignition.

## 2.1 Baseline geometry

The baseline test geometry is a 20 mm-diameter spherical volume of explosive, surrounded by a steel shell with 1 mm wall thickness. For the baseline calculation, the explosive is at 95% of its nominal density. It is convenient to account for the initial gas-filled porosity by using HE product at 293K and 0.1 MPa. The initial extent of reaction (mass fraction of product) is  $3.4 \times 10^{-5}$ . We took this to be representative of the porosity introduced by mechanical damage.

The sphere contains 7.3 g of the UK explosive at the reduced density, surrounded by an 11 g steel shell. We have taken the baseline steel strength to be 500 MPa. We note that the quasi-static burst pressure,  $P_b$ , which is the pressure that produces unlimited strain in the steel, is given in the limit of a thin-walled shell by

$$P_b = \frac{4t}{D} Y,$$

where  $t$  is the wall thickness,  $D$  is the sphere diameter, and  $Y$  is the tensile strength of the shell material. For the baseline properties, the burst pressure is 100 MPa. The baseline ignition point is the center of the sphere, and it is ignited at time zero.

## 2.2 Practical test geometry

Although convenient for calculation, the geometry described may not be practical for testing. Even if constructed as two flanged hemispheres, assembling them filled with loose powdered explosive and placing a central igniter would be a delicate affair. Perhaps a more practical geometry would be a hollow cylinder with the base plates on top and bottom sturdy enough that the release of pressure was due to the expansion of the cylindrical surface. We developed one such test geometry with a nominal burst pressure of up to 200 MPa, depending on the wall thickness. The application was the Scaled Thermal Explosion eXperiment series [2]. The design has been constructed and tested in both 25 and 50 mm diameters. Alternatively, a hemisphere with a base plate could be constructed using techniques developed for igniter and Electric Bridge Wire (EBW) detonator experiments. That geometry is also suggestive that simulations of the ignition train may be additional applications for the models being developed here. In addition, such experiments might be an additional source of data for testing models and calibrating model parameters.

## 2.3 Relationship between quasi-static burst pressure and peak pressure

The dynamic HEVR pressure history, although much slower than the energy release rate of a detonation, can be more rapid than the dynamic response time of the containment vessel. For our baseline geometry, the fundamental (elastic) period of the hollow sphere is about 8  $\mu$ s, and for geometrically scaled spheres is proportional to the diameter. In the limit of rapid pressure rise, the expansion of the confinement is limited

by inertia, not strength of materials. As a result, the peak pressure experienced in the HEVR is not simply related to the quasi-static burst pressure.

In some cases, the dynamics of the interaction can be quite interesting and complicated. In one of our calculations, the expansion of the steel confinement dropped the pressure so much that the shell, although expanded and thinned, was able to slow down and stop. This slow down, in turn, put a compression into the burning explosive, which helped the pressure in the center rise again, so accelerated the mass burning rate and re-expanded the shell.

### **3. Calculation of the spread of ignition**

Once ignition occurs, hot gas from the ignition site expands through the surrounding porous, damaged, but unlit explosive. The speed of propagation cannot exceed the sound speed of the hot gas, which is about 1 km/s. The criterion for ignition will require the hot gas to be in contact with the solid for a long enough time that the surface can be raised to the ignition temperature. Since the product species in the gas can react with the solid [3] the actual ignition temperature may be less than the ignition temperature when heated by a hot but inert gas. For our initial calculations, we assume that both the tortuosity of the path and the delay time can be represented by an effective slow-down of the propagation velocity. Our baseline calculations use the value 300 m/s for the velocity of ignition spread.

Although the velocity of ignition spread is subsonic, we have assumed for simplicity that the time of ignition can be calculated from the undeformed geometry. There is, in fact, little distortion of the baseline computational test vehicle. Figure 1 shows the geometry of the baseline test vehicle at time zero, and at 34  $\mu$ s, which is the time required for the ignition front to reach the inner wall of the steel. The calculations here were all performed with CORVUS, an AWE two-dimensional Lagrange code [4].

### **4. Calculation of pressure**

In most studies of the Deflagration to Detonation Transition, DDT, the stress in the mixture is partitioned into the gas pressure, the solid pressure, and the stress in the solid particles due to stress bridging in the skeleton [5, 6]. In the rock and soil mechanics literature, the matrix stress in the solid skeleton that is greater than the stress in the intervening fluid (water) is called the effective pressure. The shear resistance of the skeleton depends on that parameter. If the pressure in the fluid equals or exceeds the pressure in the skeleton, the particles lose contact, and the shear resistance is nil. In our initial studies, we have ignored the shear strength of the matrix. The overall resistance to consolidation offered by the matrix is a modest multiplier of the shear strength of the full density material until the last stages of densification, when the multiplier can reach 10 or more.

Another potentially important feature of the resistance of the matrix is its irreversibility. The unloading from a consolidated state has a relatively steep modulus, approaching that of the solid. In the earlier studies of DDT, the emphasis was on proceeding to detonation, not failure to detonate. As a result, the loading was substantially monotonic, and the omission of steep unloading curves in some of the studies, with the accompanying omission of unloading waves that overtake the loading

waves, was probably unimportant. In our work on HEVR, the unloading may be significant. As a result, we have chosen a method that provides such asymmetry.

Temperature equilibrium is not achieved. The flame front, which is the gas and solid interface, is thin relative to the fragment dimension. As a result, most of the solid is at the initial temperature, not the temperature of the hot gas, which is about 3000K. To determine the energy partition between gas and solid, we use the method described in [7]. In that method, the solid is on its adiabat and the gas gets the energy that is left over.

#### 4.1 Equation of state of the solid

We use the JWL form [8] for the solid equation of state, and a constant specific heat of the solid for calculating what is at best an advisory temperature. For the purpose of hydrocode simulations, the energy-dependent form may be preferred. The pressure,  $P$ , is given in terms of the relative volume,  $V$ , which is defined as  $\rho_0/\rho$ :

$$P = A \left(1 - \frac{\omega}{RV}\right) \exp(-RV) + B \left(1 - \frac{\omega}{SV}\right) \exp(-SV) + \omega e \rho$$

where  $\rho$  is the density,  $\rho_0$  the reference density,  $e$  the specific energy density, and  $A$ ,  $B$ ,  $R$ ,  $S$ , and  $\omega$  are parameters. Conventionally, the parameter  $B$  is negative when describing solids. The solid temperature can be calculated by

$$T = \left[ e - \frac{A}{R\rho_0} \exp(-RV) - \frac{B}{S\rho_0} \exp(-SV) \right] / c_v$$

where  $c_v$  is the specific heat of the solid. The  $B$  coefficient depends on the initial state of the solid, which is convenient to specify by the initial pressure and temperature,  $P_0$ ,  $T_0$  at the reference density ( $V = 1$ ). In that case the  $B$  coefficient is given by

$$B = \left[ P_0 - A \exp(-R) - \omega c_v \rho_0 T_0 \right] \exp(S)$$

and the initial energy density is given by

$$e_0 = \left[ \frac{A}{R} \exp(-R) + \frac{B}{S} \exp(-S) \right] / \rho_0 + c_v T_0$$

#### 4.2 Equation of state of the gas

We developed an equation of state table for the gas products [1] using Cheetah [9,10]. The table is rectangular, with 41 density columns and 11 temperature rows. The density entries are spaced logarithmically, except near the density of 1.0 g/cc and higher, where they are linearly spaced. The density range of the table is  $10^{-3}$  to 3 g/cc, and the temperature range is 250 to 10,000K. At temperatures of 10,000K and above, ionization effects in the gas begin to play a role. The version of Cheetah we have used (Cheetah 4) does not include such effects. It is better, however, to have an approximate value, rather than use extrapolation. Compressions in the un-ignited material can drive the gas temperature up substantially. In our computations reported here, we found that the gas would occasionally undergo excursions to density as low as  $10^{-4}$  and temperatures as high as 20,000K. We would recommend extending the table to  $10^{-5}$  g/cc and 50,000K for future versions of the model. Interpolation in the table is linear in the logarithm of density, linear in temperature and energy density, and logarithmic in pressure. The method of interpolation for an entry in density and energy density follows. The density list is searched to find the adjacent entries  $lr_1$  and  $lr_2$  where  $lr_1 \leq lr < lr_2$ . Here  $lr$  is the logarithm of the density. The linear interpolation parameter,  $p$ , is given by

$$p = \frac{lr - lr_1}{lr_2 - lr_1}.$$

The left temperature-like interpolation parameter,  $q_l$  is given by

$$q_l = \frac{e - e_{b1}}{e_{l1} - e_{b1}}, \text{ where } e_{b1} \leq e < e_{l1}$$

The parameter  $q_2$  is found similarly along the adjacent higher density column. The temperature is interpolated on the left column,  $T_l$  by

$$T_l = T_{b1}(1 - q_l) + T_{l1}q_l$$

and similarly on the right. The log of pressure,  $lp$ , is similarly interpolated on the left and right. Finally, the temperature is interpolated by

$$T = T_1(1 - p) + T_2p$$

and the log pressure interpolated similarly.

### 4.3 Model to calculate the stress in the matrix

The solid skeleton is an assembly of particles touching on some of their surfaces. Compression of that skeleton is accompanied by a rearrangement of the particles that produces an irreversible compaction, and an increasing resistance to further consolidation. An unloading-reloading path that has a higher modulus than the consolidation limit provides irreversibility. We developed a model [11] that describes this irreversible consolidation and includes explicitly the reference state porosity. If the burning process reduces the mass from the available surfaces of the particles, and they do not rearrange themselves, then the porosity (the fraction of the total volume not occupied by solid material) increases with the extent of reaction,  $\lambda$ .

$$\varphi = \phi_g = \lambda \frac{v_g}{v_0} = 1 - \phi_s = 1 - \frac{v_s(1 - \lambda)}{v_0}.$$

Here  $\varphi$  is the porosity,  $\phi_{s,g}$  the volume fractions of solid and gas,  $v_{s,g}$  are the specific volumes of the solid and gas at the initial pressure, and  $v_0$  is the initial specific volume. The relative volume,  $V_x$ , of that configuration is given by

$$V_x = \frac{v_0 \rho_{s0}}{(1 - \lambda)}$$

where  $\rho_{s0}$  is the initial density of the solid. At the relative volume  $V_x$ , the original configuration is unstressed.

The resistance to consolidation is given by a hysteretic volume dependent term and an energy dependent term,

$$P = P_c(V, V_x) + \Gamma' e \rho$$

The resistance to consolidation,  $P_c$  is given by

$$P_c = K(1/V_s - 1)$$

where  $K$  is the bulk modulus of the solid, and

$$V_s = \frac{x - \sqrt{x^2 - 4(1 - \beta)V}}{2(1 - \beta)},$$

where the parameter  $\beta \ll 1$  increases with the strength of the solid material [11], and

$$x = 1 + \beta(V_x - 1) + V(1 - \beta).$$

The unload-reload modulus,  $K'$ , is given by

$$K' = K \left( 1 - \frac{1/V - 1}{1/V_x - 1} \right),$$

and is limited to be no greater than  $K$  and no less than a specified fraction (typically 10%) of  $K$ . The hysteretic volume consolidation is augmented by a modified Gruneisen parameter where

$$\Gamma' = \left( \frac{V}{V_s} \right)^2 \frac{1 - V_s}{1 + V - 2V_s} \Gamma$$

where  $\Gamma$  is the Gruneisen parameter of the solid. The parameter values used in the calculations are given in Table 1.

We have illustrated the resistance curve to consolidation from an initial porosity of 16.7% in Figure 2, including intermediate load-unload curves. The initial relative volume is 1.2 at that porosity. At some porosity, on the order of 40%, (relative volume 1.65) the matrix can no longer support any stress because the particles no longer touch, and the matrix pressure is considered zero. Since, in our view, the damaged material is broken, we do not permit the matrix stress to be tensile. A history variable is set when the matrix over expands, so that recompression is not resisted until the previous density at zero pressure is reached. This is consistent with the view that the expanding assembly does not rearrange itself to maintain contact between the particles, but rather separates as isolated fragments. It should be noted that the pressure, calculated in this model [11] is that appropriate for the macroscopic stress acting on a plane. This macroscopic matrix pressure,  $P_{mm}$ , is given by

$$P_{mm} = \phi_s P_m$$

where  $P_m$  is the matrix stress.

#### 4.4 Calculation of the mixture stress

In hydrocode simulations, energy conservation for some specific equation of state forms can be solved directly [12]. With more general equation of state forms, the energy equation can be solved with 2-step energy iteration. This method is sufficiently accurate [13] provided that the volume change in any computational cycle is limited to about 4%. In compression, that limit corresponds to the limit imposed by the stability criterion for artificial viscosity. The iteration for a given element with a single material

$$e_h = e_o - (P_o + Q_h)(v_n - v_o)$$

$$P_h = f(v_n, e_h)$$

$$e_n = e_o - \left[ \frac{1}{2}(P_o + P_h) + Q_h \right] (v_n - v_o)$$

$$P_n = f(v_n, e_n)$$

where  $Q$  is the artificial viscosity used in hydrocodes to spread a shock discontinuity over several computational elements, and to increase the entropy appropriately across a shock front. The subscripts  $o$ ,  $n$ , and  $h$  refer to the time centering of old, new, and halfway between. The method of partitioning the energy between the gas and solid species described by [7] is to force the solid to be on its adiabat, and to allot the remaining energy to the gas. The process comprises two steps. The first step is to equilibrate pressure with the old composition, tracked by the extent of reaction,  $\lambda$ . The parameter  $\lambda$  is the mass

fraction of gas in a given computational element. Conservation of energy for the mixture requires that at each step,

$$de = -(P + Q)dv$$

with the appropriate centering. The pressure of the mixture is given by

$$P = \phi_s P_s + (1 - \phi_s) P_g.$$

Pressure equilibrium requires that

$$P_s = P_g + P_m$$

where the subscripts  $s$ ,  $g$ , and  $m$  refer to solid, gas, and matrix. Substituting the expression for the solid pressure in the equation for the change of energy in the mixture gives

$$de = -[\phi_s (P_g + P_m) + (1 - \phi_s) P_g + Q] dv$$

Expanding  $dv$  into the solid and gas parts results in

$$de = -(P_g + Q) \lambda dv_g - (P_g + Q) (1 - \lambda) dv_s - \phi_s P_m dv$$

We then identify the energy change in the gas as

$$de_g = -(P_g + Q) dv_g$$

Since the matrix specific volume is given by

$$v_m = v / (1 - \lambda)$$

we recognize that the energy change in the matrix is given by

$$de_m = -\phi_s P_m dv_m = -P_{mm} dv_m$$

The energy change in the solid is given by

$$de_s = -(P_s - P_m + Q) dv_s$$

so that the overall energy balance is given by

$$de = \lambda de_g + (1 - \lambda) (de_s + de_m)$$

At small extent of reaction, the gas specific volume change can be large, although the other volume changes are small. As result, it may be more accurate to solve for the change in the gas specific energy by

$$de_g = [de - (1 - \lambda) (de_m + de_s)] / \lambda$$

which is in keeping with the method of isochoric burn.

The first step in the calculation is to calculate the pressure and energy density at half time. We first solve

$$e_h = e_o - (P_o + Q_h) (v_n - v_o)$$

$$v_{mh} = v_n / (1 - \lambda_o)$$

$$e_{mh} = e_{mo} - \phi_{so} P_{mmo} (v_{mh} - v_{mo})$$

$$P_{mmh} = f_m (v_{mh}, e_{mh})$$

We then select a trial value for the gas specific volume,  $v_{ga}$

$$\begin{aligned}
v_{sa} &= (v_n - \lambda_o v_{ga}) / (1 - \lambda_o) \\
\phi_{sa} &= (1 - \lambda_o) v_{sa} / v_o \\
e_{sa} &= e_{so} - (P_{so} - P_{mmo} / \phi_{sa} + Q_h)(v_{sa} - v_{so}) \\
P_{sa} &= f_s(v_{sa}, e_{sa}) \\
e_{ga} &= [e_h - (1 - \lambda_o)(e_{sa} + e_{mh})] / \lambda_o \\
P_{ga} &= f_g(v_{ga}, e_{ga}) \\
F_a &= P_{ga} + P_{mmh} / \phi_{sa} - P_{sa} \Rightarrow 0
\end{aligned}$$

where the iteration requires the figure of merit  $F_a$  to be adequately close to zero. The starting guess for the gas specific volume is to assume that the solid stays at its previous value, and the gas takes up all of the volume change. For our purposes, convergence is defined as achieving the absolute value of  $F_a$  less than  $10^{-5} P_s$ , or less than 10 Pa. At the end of the iteration, the half-time values are given by

$$\begin{aligned}
v_{sh} &= v_{sa} \\
v_{gh} &= v_{ga} \\
\phi_{sh} &= (1 - \lambda_o) v_{sa} / v_n \\
P_h &= \phi_{sh} P_{sa} + (1 - \phi_{sh}) P_{ga}
\end{aligned}$$

A second iteration for the pressure,  $P_t$ , uses the energy density  $e_t$  based on the half time pressures. For this iteration the starting gas volume,  $v_{gb}$ , is the previous equilibrium value.

$$\begin{aligned}
e_t &= e_o - \left[ \frac{1}{2} (P_o + P_h) + Q_h \right] (v_n - v_o) \\
v_{mt} &= v_{mn} = v_n / (1 - \lambda_o) \\
e_{mt} &= e_{mo} - \left[ \frac{1}{2} (P_{mmo} + P_{mmh}) \right] (v_{mt} - v_{mo}) \\
P_{mmt} &= f_m(v_{mt}, e_{mt})
\end{aligned}$$

A trial value for  $v_{gb}$  is selected for the next iteration

$$\begin{aligned}
v_{sb} &= (v_n - \lambda_o v_{gb}) / (1 - \lambda_o) \\
\phi_{sb} &= (1 - \lambda_o) v_{sb} / v_n \\
e_{sb} &= e_{so} - \left[ \frac{1}{2} (P_{so} + P_{sh} - P_{mmo} / \phi_{sh} - P_{mmh} / \phi_{sb}) + Q_h \right] (v_{sb} - v_{so}) \\
P_{sb} &= f_s(v_{sb}, e_{sb}) \\
e_{gb} &= [e_t - (1 - \lambda_o)(e_{sb} + e_{mt})] / \lambda_o \\
P_{gb} &= f_g(v_{gb}, e_{gb}) \\
F_b &= P_{gb} + P_{mmt} / \phi_{sb} - P_{sb} \Rightarrow 0
\end{aligned}$$

After successful iteration, the values are saved as the trial state. The final step is to update the extent of reaction at constant volume. The total energy remains the same. The change in the extent of reaction for each computational element is given by

$$\frac{d\lambda}{dt} = \frac{6}{d} (1-\lambda)^{2/3} v_f \left[ \frac{\max(p, 0.1 \text{ MPa})}{p_0} \right]^n$$

where  $p_0 = 1 \text{ GPa}$ ,  $v_f = 1 \text{ m/s}$ , and  $n = 1$  [1]. The parameter  $d$  is the diameter of a sphere with the local surface-to-volume ratio. The iteration for pressure proceeds as follows with the new extent of reaction:

$$e_n = e_t$$

$$v_{mn} = v_n / (1 - \lambda_n)$$

$$e_{mn} = e_{mo} - \left[ \frac{1}{2} (P_{mmt} + P_{mmo}) \right] (v_{mn} - v_{mo})$$

$$P_{mmm} = f_m(v_{mn}, e_{mn})$$

A value of the gas specific volume  $v_{gc}$  is selected, and the iteration for the new extent of reaction proceeds.

$$v_{sc} = (v_n - \lambda_n v_{gc}) / (1 - \lambda_n)$$

$$\phi_{sc} = (1 - \lambda_n) v_{sc} / v_n$$

$$e_{sc} = e_{st} - (P_{st} - P_{mmt} / \phi_{sc}) (v_{sc} - v_{st})$$

$$P_{sc} = f_s(v_{sc}, e_{sc})$$

$$e_{gc} = [e_n - (1 - \lambda_n)(e_{sc} + e_{mn})] / \lambda_n$$

$$P_{gc} = f_g(v_{gc}, e_{gc})$$

$$F_c = P_{gc} + P_{mmm} / \phi_{sc} - P_{sc} \Rightarrow 0$$

For this last iteration, the starting solid specific volume is assumed not to change from the previously converged value of  $v_{st}$ . After successful completion of the iteration, the new values are updated. Although in this last step, the gas and solid are calculated as increments from the trial state, the matrix is recalculated from the old state. The reason is that the matrix would always be unloading from the trial state to the new extent of reaction. The extent of reaction always increases, so the value  $v_{mn}$  is always greater than  $v_{mt}$ . This would always leave the matrix in an unload-reload state below the crush curve.

$$\phi_{sn} = (1 - \lambda_n) v_{sn} / v$$

$$P_n = \phi_{sn} P_{sc} + (1 - \phi_{sn}) P_{gc}$$

$$e_{xn} = e_{xc}$$

$$v_{xn} = v_{xc}$$

$$P_{xn} = P_{xc}$$

where the subscript  $x$  stands for  $s$  and  $g$ . In our implementation, all three iterations are performed with a simple Newton solver,

$$v_{g,j+1} = v_{g,j} - F_j (v_{g,j} - v_{g,j-1}) / (F_j - F_{j-1}).$$

Here  $j$  is used as an iteration counter. At all steps in the iteration, the gas specific volume is constrained to be more than a minimum value that corresponds to the maximum density in the table. In addition, the solid specific volume is constrained to be less than the specific volume at which the zero-temperature pressure-volume isotherm has a minimum. At extreme values of the extent of reaction, the specific volumes in the

iteration can exceed these values. If a limit is exceeded, the value chosen is midway between the most recent value and the limit.

In our implementation, we found that in certain circumstances the unburned explosive was subjected to a strong rarefaction, which decoupled the matrix, followed by a recompression that heats the gas strongly. In some cases, the iteration to achieve pressure equilibrium did not converge. In those circumstances, reducing the time step permitted convergence. In other circumstances, the pressure was observed to oscillate significantly. This is a common occurrence for porous materials. The standard artificial viscosity forms do not produce enough entropy to increase the internal energy across a shock front in a porous solid. The additional energy is manifest by ringing behind the shock front, as an additional kinetic energy. Increasing the artificial viscosity coefficients suppresses that ringing, and in some cases can improve convergence.

## **5. Results for computational test vehicle**

### **5.1 Results for the baseline geometry**

For the baseline case, the pressure histories in cells at  $x=0$  and original  $y$ -coordinates of 4.6, 6, 7.6, and 9 mm show a decreasing value of peak pressure in Figure 3. Also shown there is the volume-averaged pressure, which we use in the following figures as representative of the pressure in the test vehicle. The peak of the volume-averaged pressure is about twice the static burst pressure. At smaller radii than those shown, the spherical convergence from a reflection off the steel interface increases the peak pressure. With the mesh shown, the pressure at the ignition point increases to over 2 GPa at a time of 40  $\mu$ s. This peak pressure spike, about 10 times the nominal pressure maximum, is mesh-size dependent, and also dependent on the high symmetry of the baseline test geometry. For the baseline case about 0.4 g of the initial 7.3 g is burned before the case expands and would ultimately break.

The matrix stress is relatively unimportant for the baseline computational test vehicle. The matrix is somewhat compressed away from the ignition zone, but once the ignition front passes the matrix begins to burn, loses contact, and the matrix stress drops to zero. In deflagration to detonation transition (DDT) testing and simulations with similar models, the strong confinement and planar ignition sends a strong compression into the unburned material. In our geometry, the compression from the ignition point is subject to spherical divergence.

### **5.2 Effect of various parameters**

The velocity of the ignition front affects the time of peak pressure, but not its value. See Figure 4 where the ignition front velocity is dropped from 300 to 100 m/s. The mass burned (Figure 5) is essentially unchanged.

The location of the ignition point at  $y=0$ ,  $x=0$ , -5, -8, and -10 mm, has little effect on the volume averaged pressure (Figure 6) and similarly little effect on the mass burned (Figure 7). As the ignition point moves farther from the center there is a tendency to concentrate the strain in the shell at the point  $y=0$ ,  $x=10$  mm, causing early failure of the containment. We increased the porosity from 5 to 35%. The latter value is typical for assemblies that are made by pouring loose powder and vibrating the container (tap density). The result is a delay in the appearance of the peak pressure (Figure 8) and a

modified value, so that the maximum pressure is associated with an intermediate porosity. The total mass burned is essentially unchanged. See Figure 9. In some sense the shell is responding to the same pressure, which is caused by burning the same mass of powder.

The strength of the confinement has a significant effect on the peak pressure (Figure 10) and the mass burned (Figure 11). Doubling the strength doubles the peak pressure and the mass burned. We notice an interesting feature of the dynamics for the strong vessel. After the peak pressure, the container expands, reducing the pressure. However, the pressure in the interior drops more quickly than the thinning wall reduces the burst pressure. By about 100  $\mu\text{s}$ , the shell stops expanding. This causes compression in the interior of the vessel, and spherical convergence causes a noticeable increase in the mass-burning rate, which raises the pressure. By 250  $\mu\text{s}$  the sphere has expanded again, and begins to reduce the pressure in the HE. If we double the surface area of the explosive, the peak pressure does not change much (Figure 12) but it is sustained longer, so that the mass burned is nearly double. We note that a geometrically scaled vessel with twice the diameter but the same specific surface area (equivalent sphere diameter) has a geometrically scaled result. The pressure, shell velocity, and extent of reaction are unchanged, although the time scale is doubled. The starting mass and the mass burned are eight times that for the smaller scale result. We ignored any rate-dependent properties. If strain-rate effects are present, the larger vessel will be slightly weaker because the strain-rate is halved. For the extreme case of 10 times the specific surface area, the peak pressure doubles to 0.4 GPa (Figure 12), and the mass burned is nearly 3 g by 50  $\mu\text{s}$ . The alternative geometric scaling with the original specific surface area but 10 times the diameter (7.3 kg) burns 3 kg in 500  $\mu\text{s}$ . The lesson here for HEVR is that with the same specific surface area, large volumes are more dangerous than small volumes. Not only is a larger mass of explosive present, but also a larger fraction of the explosive is burned in a relatively shorter time.

### **5.3 Deflagration to Detonation Transition (DDT)**

The phenomenon of DDT is a possible outcome of HEVR, and our models need to identify the circumstances when it occurs, and when it does not. If the ignition front propagates more slowly than a compression shock in the unburned but damaged explosive, then a detonation model such as CREST [14] will be valuable. That model accounts for the effect of porosity on the run to detonation, and can distinguish the effect on initiation of pressure from a shock and the same pressure from an adiabatic compression. We note that data on the lower bound of shock pressure for initiation, such as is used in the James criterion for detonation [15] as a function of porosity is lacking for most explosives. We have performed a one-dimensional calculation with the initiation near the end of an unyielding tube filled with 500  $\mu\text{m}$  particles at 5% porosity. Pressure histories are recorded at 50 mm intervals down the length of the tube (Figure 14). They show a strengthening and accelerating shock propagating down the tube. Experiments with the UK explosive [16] show that 2 GPa shocks result in a run to detonation length of 35 mm. Although data are lacking for damaged, porous explosive, and for shock pressures much less than 2 GPa, it seems clear that a detonation would occur at a location about 300 mm down the tube. Calculations with the same geometry using twice the

specific surface area or half-diameter (250  $\mu\text{m}$ ) particles show similar results, except that the detonation point is located much closer to the ignition source.

In HEVR events, the ignition is started in a small volume of material that is the most strongly deformed. As a result, the compression wave that emanates from this volume decays in amplitude with spherical divergence. In standard DDT tests, the porous explosive is contained in a strong metal pipe, and the initiation is planar. The lack of substantial loss in the pressure wave means that as the pressure builds in the initiation volume, compression waves can catch up to the shock front and strengthen it. This geometry permits a shock initiation in material that has not yet been ignited at some distance down the tube, away from the initiation site.

In HEVR events, reflections from nearby metallic surfaces are unlikely to show constructive interference and amplification. Our baseline geometry, however, has spherical symmetry so the ignition point is strongly recompressed. The recompression is probably not a shock, and it occurs in material that is burning. The finite compressibility of the hot gas inhibits consolidation of the matrix that may occur when burning is not achieved. Hot spots associated with the heterogeneous consolidation of a porous explosive may not occur. Mesoscale simulations coupled with experiments would give insight into the possible initiation mechanisms at work in the strong compression of burning explosive.

## 6. Summary

We have developed a burn model for HEVR that incorporates porosity, specific surface area, and propagation of an ignition. It calculates the resulting build-up of pressure. In DDT geometry, where the ignition volume is a planar disk, and the wave propagation is essentially one-dimensional planar, the model exhibits a build-up of pressure in the ignited volume, and the propagation of a strengthening shock in the unburned explosive. That shock wave can lead to a detonation that starts part way down the tube, referred to as a retonation.

The model described here is the first, required step in developing a comprehensive, interactive model, which uses the damaged surface area, porosity, and ignition time and location described previously [1]. The comprehensive model, then exhibits element-by-element varying properties that affect flame propagation and pressure build-up. The basis for that model has been described here.

## 7. References

1. J.E. Reaugh, "Progress in model development to quantify High Explosive Violent Response (HEVR) to mechanical insult," LLNL-TR-405903, August 2008.
2. J.F. Wardell, J.L. Maienschein, "The Scaled Thermal Explosion Experiment," *Proceedings, 12<sup>th</sup> International Detonation Symposium*, San Diego, CA, August 2002.
3. Behrens, R.; Maharrey, S., Chemical and Physical Processes that Control the Thermal Decomposition of RDX and HMX. In *Combustion of Energetic Materials*, Kuo, K. K.; DeLuca, L. T., Eds. Begell House: New York, 2002; pp 3 - 21.
4. A.J. Barlow, "Friction in CORVUS, a 2D ALE code," in *Proceedings, 22<sup>nd</sup> International Symposium on Shock Waves*, London, 1999 ed. G.J. Ball et al., (Southampton, Univ. of Southampton) p653.

5. M.R. Baer, J.W. Nunziato, "A two-phase mixture theory for the deflagration-to-detonation transition (DDT) in reactive granular materials," *Int. J. Multiphase Flow*, **12** (6) p861-889, 1986.
6. A.K. Lapela, R. Menikoff, J.D. Bdzil, S.F. Son, D.S. Stewart, "Two-phase modeling of deflagration-to-detonation transition in granular materials: Reduced equations," *Physics of Fluids*, **13** (10) p3002-3024, October 2001.
7. J.E. Reaugh, E.L. Lee, "Isochoric burn, an internally consistent method for the reactant to product transformation in reactive flow," *Proceedings, 12<sup>th</sup> International Detonation Symposium*, San Diego, CA, August 2002.
8. E.L. Lee, H.C. Hornig, "Equation of state of detonation product gases," UCRL-70809, *12<sup>th</sup> International Symposium on Combustion*, Potier, France, 1968.
9. L.E. Fried, W.M. Howard, P.C. Souers, "EXP6: A new equation of state library for high-pressure thermochemistry," *Proceedings, 12<sup>th</sup> International Detonation Symposium*, San Diego, CA, August 2002.
10. S. Bastea, K. Glaesmann, and L.E. Fried, "Equations of state for high explosive detonation products with explicit polar and ionic species," *Proceedings, 13<sup>th</sup> International Detonation Symposium*, Norfolk, VA, July 2006.
11. J.E. Reaugh, "Computer simulations to study the explosive consolidation of powders into rods," *J. Appl. Phys.*, **61** (3) p962-968, February 1987.
12. M.L. Wilkins, "Calculation of Elastic-Plastic Flow," in *Methods in Computational Physics, Vol. 3: Fundamental Methods in Hydrodynamics*, B. Alder, ed., Academic Press, 1964.
13. M.L. Wilkins, *Computer Simulation of Dynamic Phenomena*, Springer, 1999.
14. C.A. Handley, "The CREST reactive burn model," *Proceedings, 13<sup>th</sup> International Detonation Symposium*, Norfolk, VA, July 2006.
15. H.R. James, "An Extension to the Critical Energy Criterion Used to Predict Shock Initiation Thresholds," *Propellants, Explosives, Pyrotechnics*, **21**, p8-13, 1996.
16. R.E. Winter, S.S. Sorber, D.A. Salisbury, P. Taylor, R. Gustavsen, S. Sheffield, R. Alcon, "Experimental study of the shock response of an HMX-based explosive," *Shock Waves*, **15**, (2) p89-101, 2006.

## 8. Table

**Table 1. Parameter values used in the simulations**

Use	Parameter	Value
Solid equation of state	A	69.69
	B	Calculated
	R	7.8
	S	3.9
	w	0.01
	$\rho_0$	1.842 g/cc
	$c_{vs}$	1.086 J/g
Matrix equation of state	K	18 GPa
	$\Gamma$	0.5
	$\beta$	0.001
Burn rate	d	0.5 mm
	$p_0$	1 GPa
	$v_f$	1 m/s
	n	1
Ignition velocity	$v_{ig}$	300 m/s
Vessel diameter	D	20 mm
Shell thickness	t	1 mm
Shell yield strength	Y	0.5 GPa

## 9. Figures

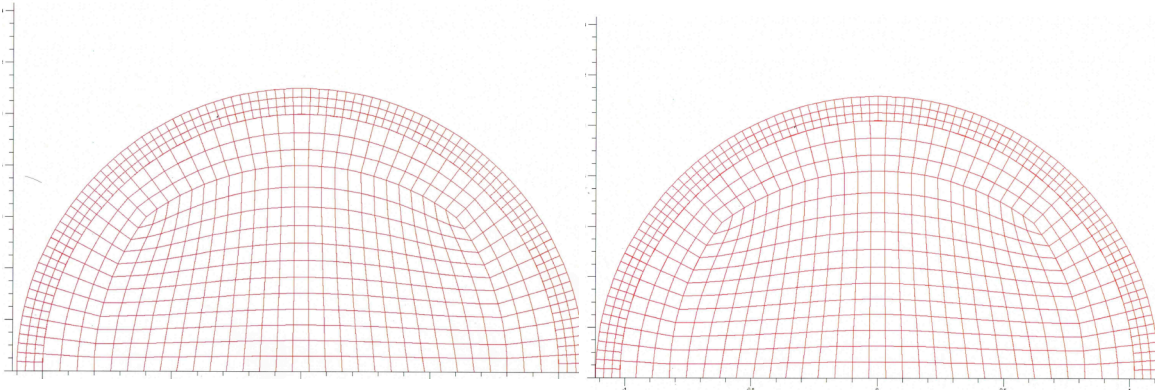


Figure 1. Axisymmetric mesh of baseline geometry at time zero (left) and at 34  $\mu\text{s}$ . The mesh has expanded slightly at this time. The baseline position of the igniter is at the center of the sphere,  $(x, y) = (0, 0)$ . There is a slideline between the explosive and the steel.

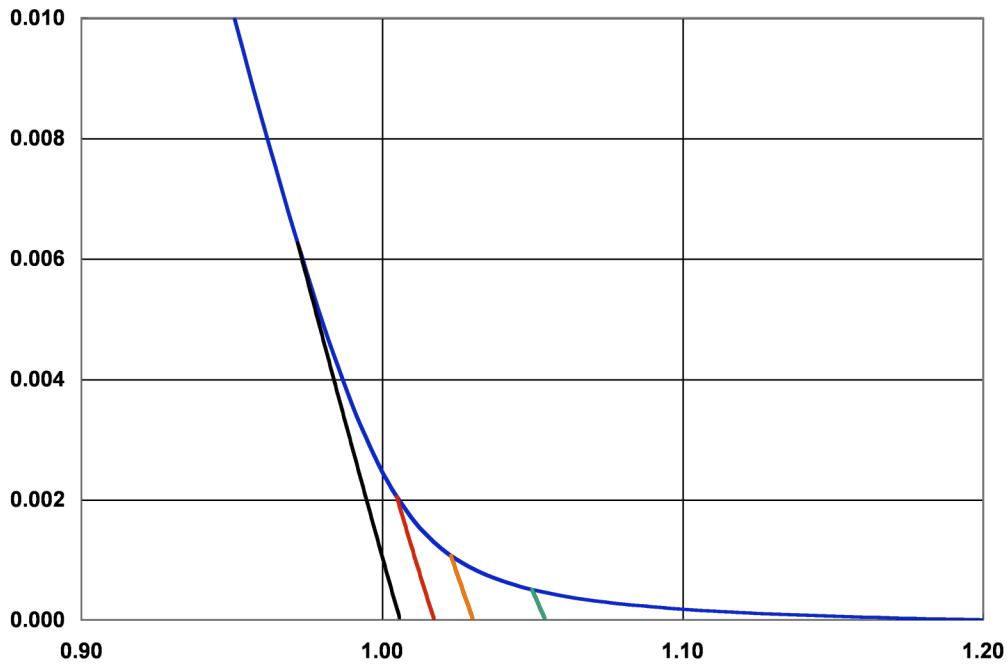


Figure 2. Compaction pressure of matrix, Mbar, as a function of relative volume. The significantly steeper load-unload traces are also shown.

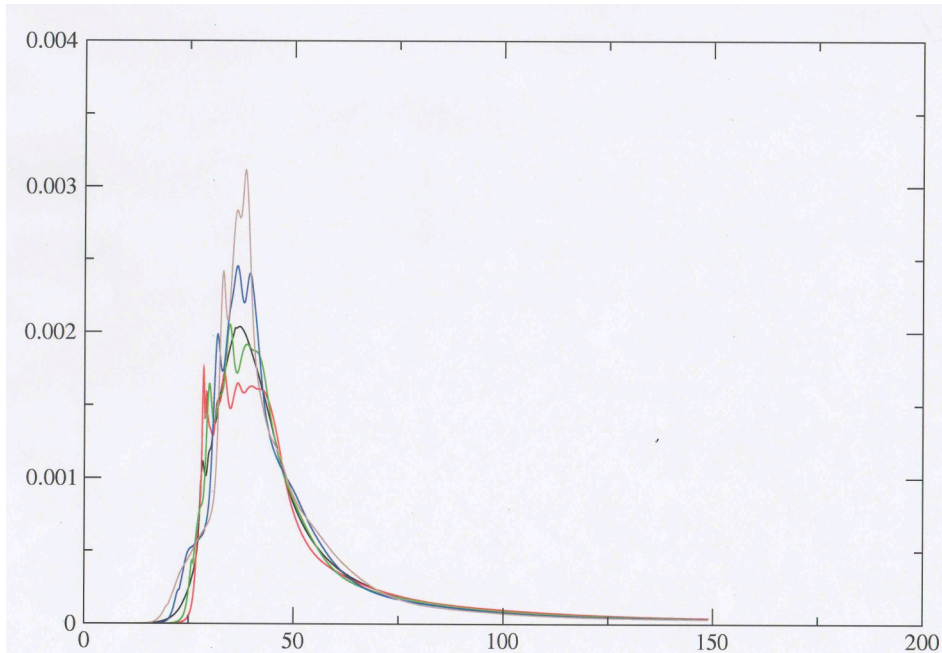


Figure 3. Pressure, Mbar, in the baseline geometry at locations (from maximum to minimum pressure at  $40 \mu\text{s}$ )  $x=0$ ,  $y=4.6$ ,  $6$ ,  $7.6$ , and  $9$  mm. The volume-average of pressure is also shown as a function of time (smooth black line).

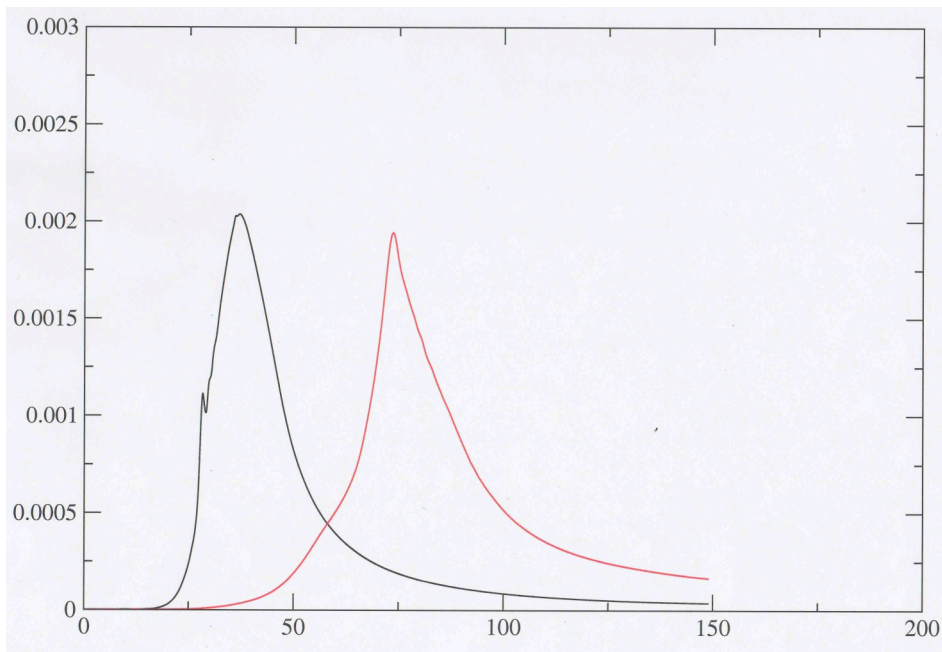


Figure 4. Volume averaged pressure, Mbar, as a function of time,  $\mu\text{s}$  for the baseline ignition velocity of  $300$  m/s (black) and for  $100$  m/s (delayed peak, red).

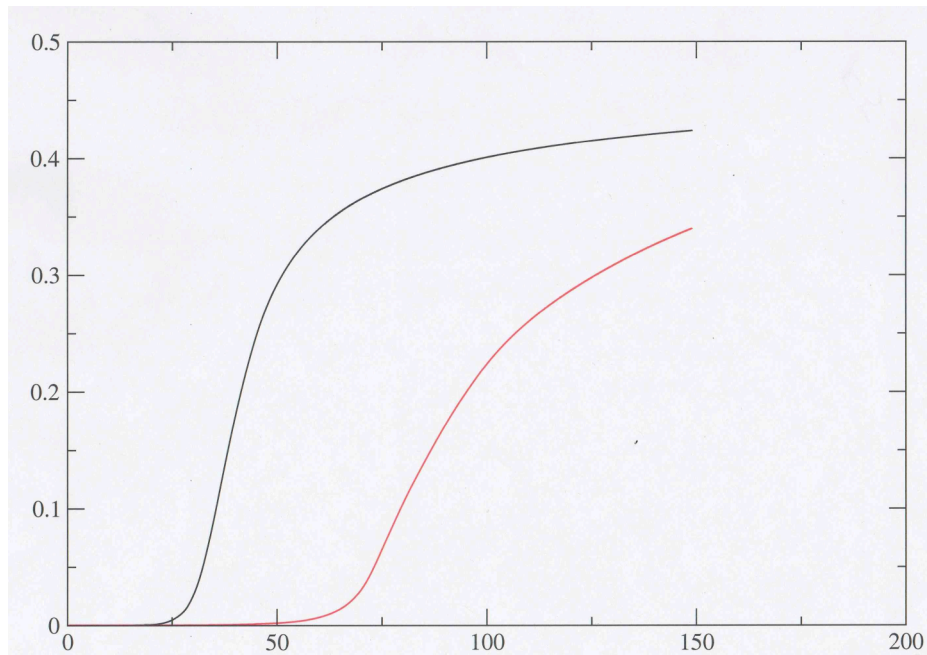


Figure 5. Mass burned, g, as a function of time,  $\mu\text{s}$ , for the baseline ignition velocity of 300 m/s (black) and 100 m/s (delayed, red)

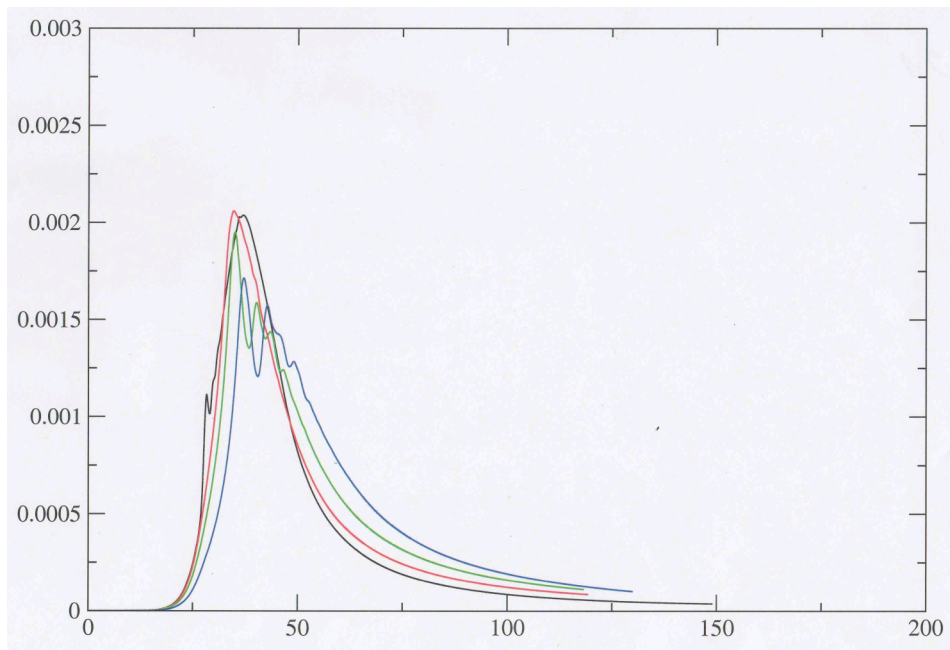


Figure 6. Volume averaged pressure, Mbar, as a function of time,  $\mu\text{s}$ , for the baseline ignition point  $x=0$  (black) and (from earliest to latest time at 0.001)  $x=-0.5$  (red),  $-0.8$  (green), and  $-1.0$  (blue).

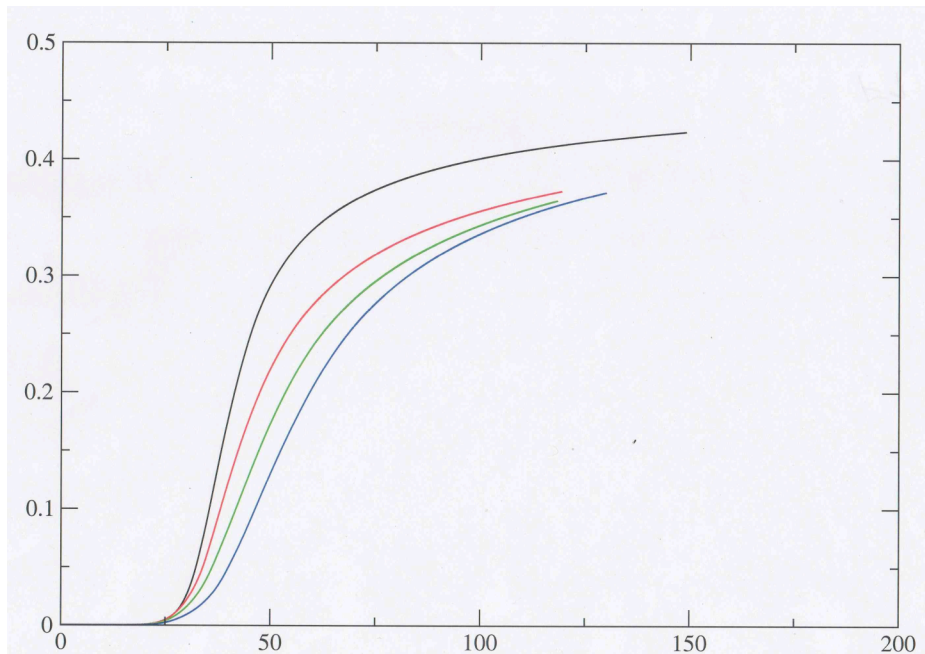


Figure 7. Mass burned, g, as a function of time,  $\mu\text{s}$  for the baseline ignition point  $x=0$ , and from earliest to latest time at 0.2,  $x=-0.5$  (red),  $-0.8$  (green), and  $-1.0$  (blue).

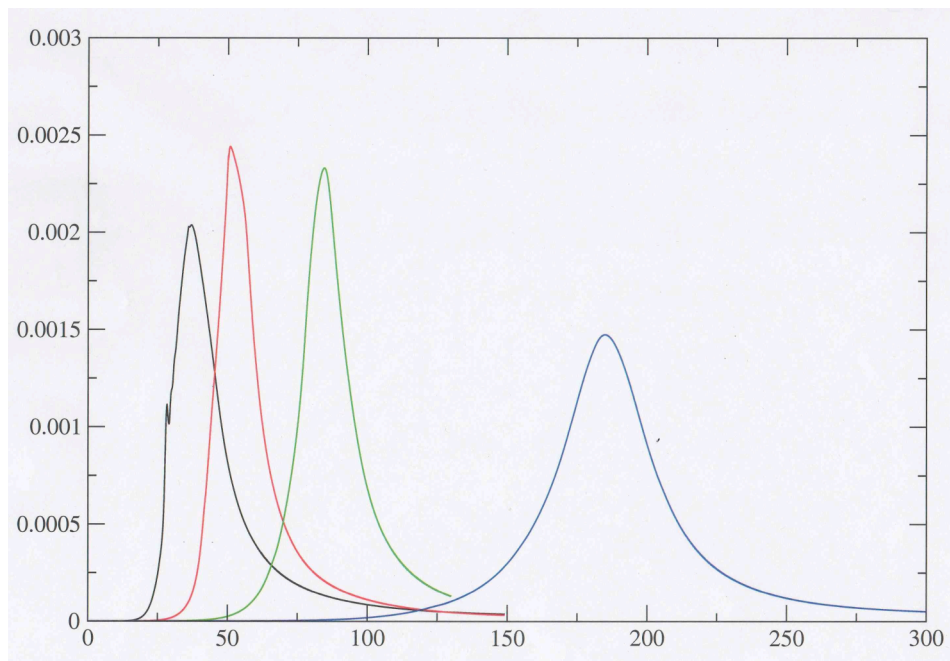


Figure 8. Volume averaged pressure, Mbar, as a function of time,  $\mu\text{s}$ , for the baseline porosity, 0.05 (black) and for increasing time of the peak values, 0.09 (red), 0.17 (green), and 0.35 (blue).

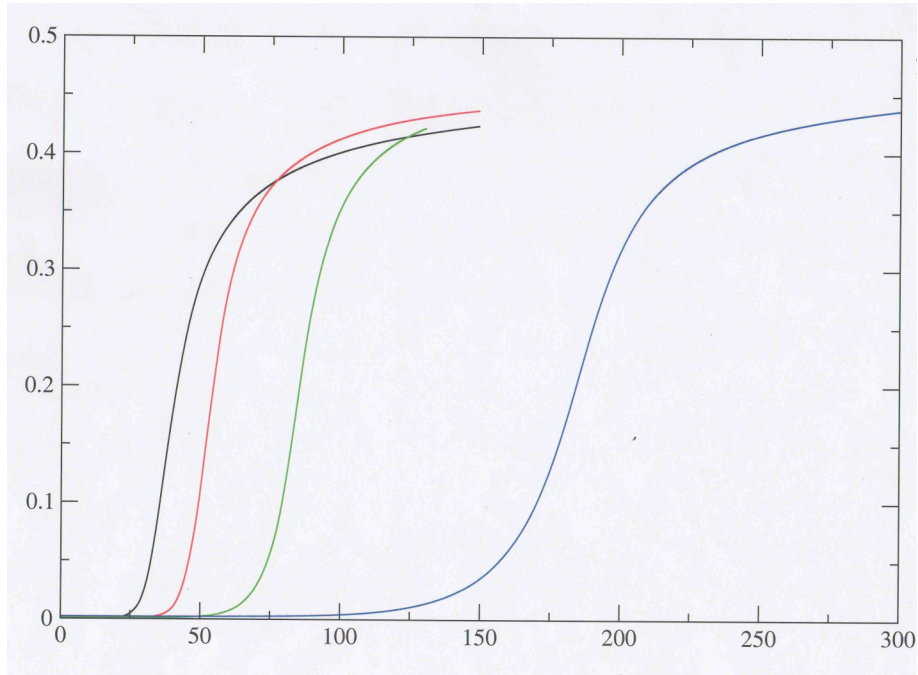


Figure 9. Mass burned, g, as a function of time,  $\mu\text{s}$ , for the baseline porosity 0.05 (black) and, at increasing times, for 0.09 (red), 0.17 (green), and 0.35 (blue).

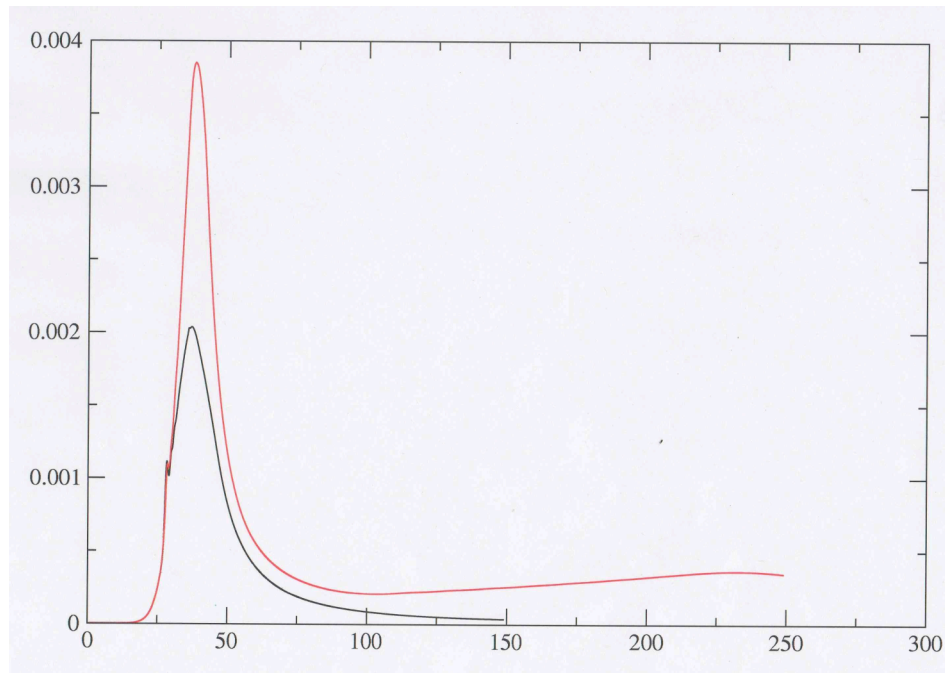


Figure 10. Volume averaged pressure, Mbar, as a function of time,  $\mu\text{s}$ , for the baseline steel strength 0.5 GPa (black) and 1.0 GPa (red, peak value 0.004).

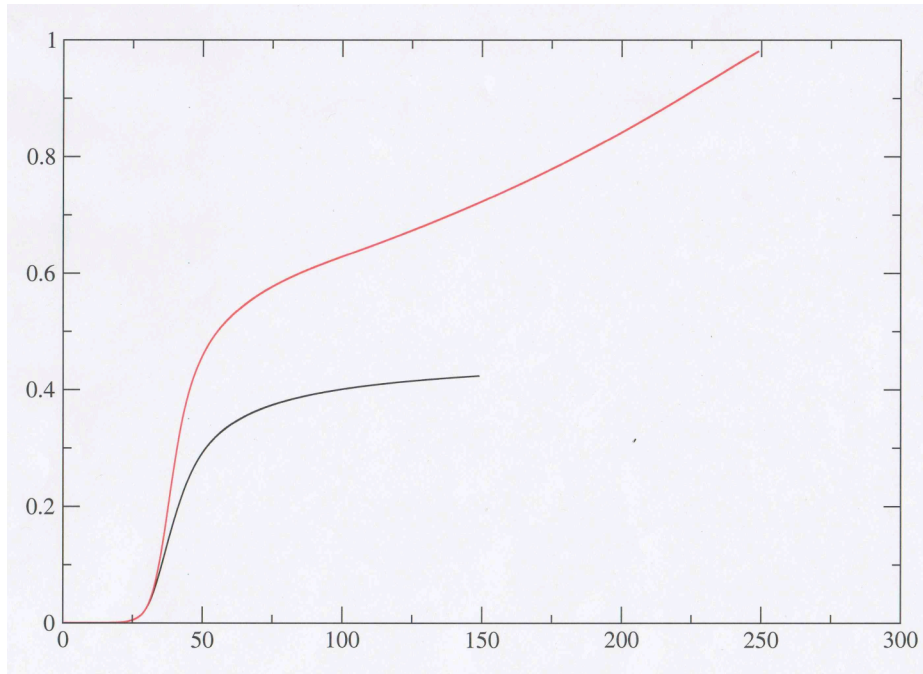


Figure 11. Mass burned, g, as a function of time,  $\mu\text{s}$ , for the baseline steel strength 0.5 GPa (black) and for 1.0 GPa (red, peak value 1).

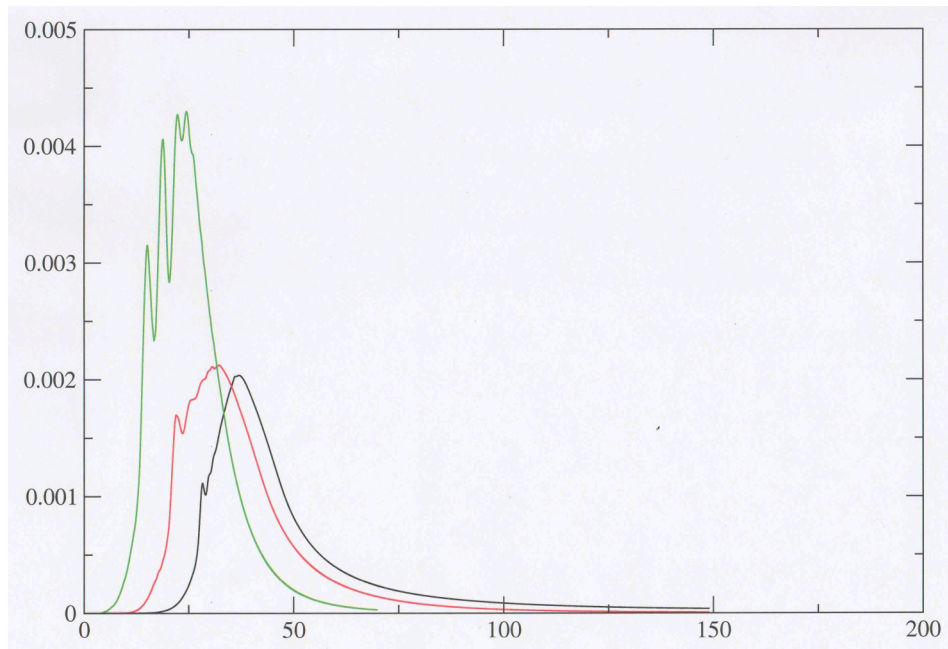


Figure 12. Volume averaged pressure, Mbar, as a function of time,  $\mu\text{s}$ , for the baseline equivalent sphere diameter 0.5 mm (black) and increasing in peak values, 0.25 mm (red), and 0.05 mm (green).

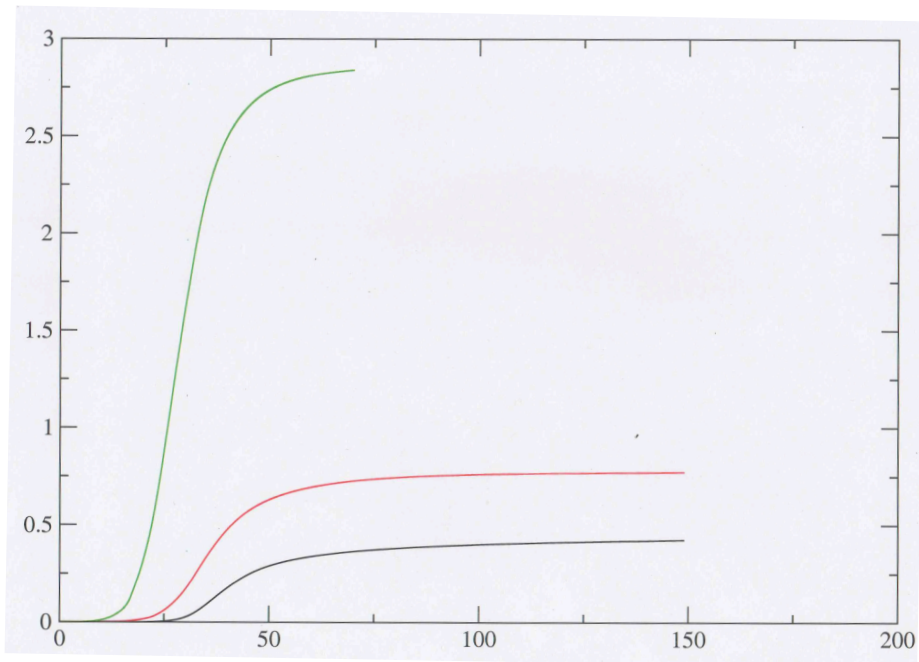


Figure 13. Mass burned, g, as a function of time,  $\mu\text{s}$ , for the baseline equivalent spheres 0.5 mm (black) and increasing in peak values, for 0.25 mm (red) and 0.05 mm (green).

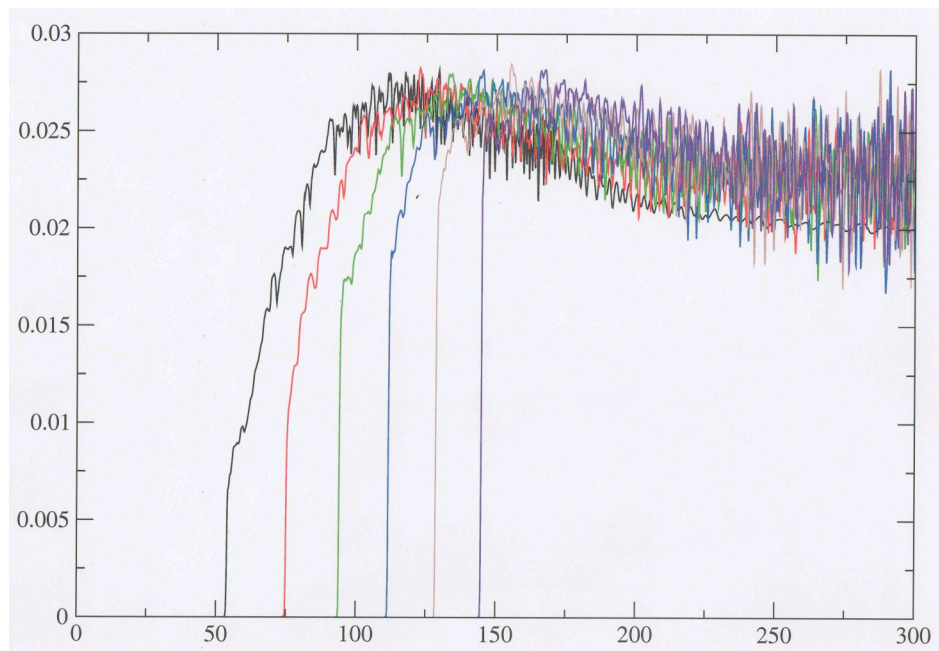


Figure 14. Pressure (Mbar) in DDT geometry as a function of time,  $\mu\text{s}$ . The histories are taken at 50 mm intervals down a one-dimensional planar tube starting at 50 mm from the planar ignition site. The shock is strengthening and accelerating down the tube.